Electrical transport, electrothermal transport, and effective electron mass in single-crystalline In_2O_3 films

Natalie Preissler and Oliver Bierwagen*
Paul-Drude-Institut für Festkörperelektronik, Hausvogteiplatz 5–7, 10117 Berlin, Germany

Ashok T. Ramu
Department of Electrical and Computer Engineering, University of California, Santa Barbara, California 93106, USA

James S. Speck
Materials Department, University of California, Santa Barbara, California 93106, USA

(Received 7 September 2012; revised manuscript received 12 June 2013; published 7 August 2013)

A comprehensive study of the room-temperature electrical and electrothermal transport of single-crystalline indium oxide (In_2O_3) and indium tin oxide (ITO) films over a wide range of electron concentrations is reported. We measured the room-temperature Hall mobility μ_H and Seebeck coefficient S of unintentionally doped and Sn-doped high-quality, plasma-assisted molecular-beam-epitaxy-grown In_2O_3 for volume Hall electron concentrations n_H from 7×10^{16} cm^{-3} (unintentionally doped) to 1×10^{21} cm^{-3} (highly Sn-doped, ITO). The resulting empirical $S(n_H)$ relation can be directly used in other In_2O_3 samples to estimate the volume electron concentration from simple Seebeck coefficient measurements. The mobility and Seebeck coefficient were modeled by a numerical solution of the Boltzmann transport equation. Ionized impurity scattering and polar optical phonon scattering were found to be the dominant scattering mechanisms. Acoustic phonon scattering was found to be negligible. Fitting the temperature-dependent mobility above room temperature of an In_2O_3 film with high mobility allowed us to find the effective Debye temperature ($\Theta_D = 700$ K) and number of phonon modes ($N_{\mathrm{OPML}} = 1.33$) that best describe the polar optical phonon scattering. The modeling also yielded the Hall scattering factor r_H as a function of electron concentration, which is not negligible ($r_H \approx 1.4$) at nondegenerate electron concentrations. Fitting the Hall-scattering-factor corrected concentration-dependent Seebeck coefficient $S(n)$ for nondegenerate samples to the numerical solution of the Boltzmann transport equation and to widely used, simplified equations allowed us to extract an effective electron mass of $m^* = (0.30 \pm 0.03)m_e$ (with free electron mass m_e). The modeled mobility and Seebeck coefficient based on polar optical phonon and ionized impurity scattering describes the experimental results very accurately up to electron concentrations of 10^{19} cm^{-3}, and qualitatively explains a mobility plateau or local maximum around 10^{20} cm^{-3}. Ionized impurity scattering with doubly charged donors best describes the mobility in our unintentionally doped films, consistent with oxygen vacancies as unintentional shallow donors, whereas singly charged donors best describe our Sn-doped films. Our modeling yields a (phonon-limited) maximum theoretical drift mobility and Hall mobility of $\mu = 190$ cm^2/Vs and $\mu_H = 270$ cm^2/V s, respectively. Simplified equations for the Seebeck coefficient describe the measured values in the nondegenerate regime using a Seebeck scattering parameter of $r = -0.55$ (which is consistent with the determined Debye temperature), and provide an estimate of the Seebeck coefficient to lower electron concentrations. The simplified equations fail to describe the Seebeck coefficient around the Mott transition ($n_{\mathrm{Mott}} = 5.5 \times 10^{18}$ cm^{-3}) from nondegenerate to degenerate electron concentrations, whereas the numerical modeling accurately describes this region.

DOI: 10.1103/PhysRevB.88.085305 PACS number(s): 72.20.Pa, 73.50.Lw, 72.20.Fr, 72.20.Dp

I. INTRODUCTION

Indium oxide, In_2O_3, is a transparent semiconducting oxide, that has been traditionally used in gas sensors or—in its highly doped form ITO (indium tin oxide)—as transparent contacts in light emitting diodes, displays, and solar cells. These conventional applications are commonly based on relatively defective, impure, and polycrystalline material with high, degenerate electron concentrations typically above 10^{19} cm^{-3}, and electron mobilities well below 100 cm^2/V s (see overview in Ref. 1). More recently, it has been recognized that In_2O_3 can become a new transparent semiconductor—if synthesized to a higher material quality and purity, and with well-defined conductivity. Based on this high quality, novel or high-performance electronic devices can be developed and the inherent material physics of In_2O_3—without side effects of excess impurities or grain boundaries—can be studied. For example, high quality, In_2O_3 bulk single crystals have been demonstrated with room-temperature (RT) nondegenerate Hall electron concentrations and related Hall mobilities of 3.5×10^{17} cm^{-3} and 160 cm^2/V s or,[2] very recently, 1.2×10^{17} cm^{-3} and 180 cm^2/V s.[1] We have demonstrated the growth of high-quality, single crystalline, thin film In_2O_3 by plasma-assisted molecular beam epitaxy[3,4] with high room-temperature Hall mobilities up to 226 cm^2/V s at nondegenerate, unintentionally doped (UID) Hall electron concentrations as low as 5×10^{16} cm^{-3}.[5] A microscopic understanding of the electron transport in In_2O_3 has so far been limited to rough, phenomenological approximations in non-degenerate samples,[2] or even the complete neglect of phonon scattering in highly degenerate samples.[6,7]

Particularly, the impact of phonons on transport (optic or acoustic, their microscopic parameters) and the effective electron mass is still not well established. The relatively low electron mobility of In_2O_3 makes it difficult to determine the electron effective mass by cyclotron resonance but does not affect the extraction of effective electron mass from measured electron concentrations and Seebeck coefficients.

The Seebeck coefficient (thermopower and thermoelectric power) S is a thermoelectric transport property, that is easy to measure and provides valuable information about a noninsulating material: the sign of S depends on the carrier type (by convention negative for electrons and positive for holes) and its magnitude is a function of the scattering mechanisms and the Fermi level, which in turn depends on the carrier effective mass m^* and the volume carrier concentration n. Hence the Seebeck coefficient can be used to determine the carrier type, the volume carrier concentration (if m^* and the scattering mechanisms are known), or m^* (if n and the scattering mechanisms are known). Estimating the volume carrier concentration can, for example, help to determine if a sheet carrier concentration extracted from Hall effect measurements is due to the carriers spread across the total sample thickness or rather due to carriers in a thin interface or surface layer—a situation that has been observed in thin film InN[8] or SnO_2[9] samples. In addition, the Seebeck coefficient is an important parameter in the figure of merit ZT, which determines the efficiency of a material for applications in thermoelectric coolers or thermoelectric power generators. While many papers have been published on the temperature dependent Seebeck coefficient of polycrystalline[10–12] and single crystalline[13,14] In_2O_3 and ITO samples at particular volume electron concentrations (mostly in the context of thermoelectric applications), reports on the In_2O_3 RT Seebeck coefficient as a function of n are limited to degenerate volume electron concentrations between 1×10^{19} cm^{-3} and 1×10^{21} cm^{-3} for bulk In_2O_3 ceramics[15] and polycrystalline thin In_2O_3 films.[16] Measured Seebeck coefficients have been compared to modeled Seebeck coefficients based on simplifications of the Boltzmann transport equation (BTE),[10,11,15–18] but which are typically restricted to being either well within the degenerate or the nondegenerate regime, the relaxation time approximation, or a parabolic conduction band. Another approach[19] numerically solves the full BTE which makes it not subject to the above mentioned restrictions and will be used in this work.

In this contribution we report a systematic, combined experimental and theoretical study of the RT electron transport properties and Seebeck coefficient of In_2O_3. The experiments are based on high quality, single crystalline In_2O_3 thin films with Hall electron concentrations from 7×10^{16} cm^{-3} up to 1×10^{21} cm^{-3}, i.e., from the—previously unexplored—nondegenerate regime up to the ITO regime at the doping limit of In_2O_3. Both electron mobility and Seebeck coefficient are consistently modeled with a numerical solution of the full Boltzmann transport equation, to clarify the main scattering mechanisms and their microscopic parameters, including the electron effective mass. The temperature dependent Hall mobility of a nondegenerate sample allowed us to determine the details of the dominant polar optical phonon scattering.

II. EXPERIMENT

A. Samples

The investigated samples consist of approximately 500 nm thick In_2O_3(001) layers grown by plasma-assisted molecular beam epitaxy on (001) oriented, insulating yttria-stabilized zirconia (ZrO_2:Y, YSZ) at an optimized substrate temperature of 650 °C and different oxygen-to-indium flux ratios.[3] The films are continuous, single crystalline, and of high structural quality.[4]

A wide range of volume electron concentrations was covered by using UID and intentionally doped samples. UID samples possess Hall volume electron concentrations up to 10^{18} cm^{-3}, which could be decreased to values as low as 7×10^{16} cm^{-3} by annealing in an oxygen atmosphere at 750 °C for 60 s.[5] Higher Hall volume electron concentrations up to 10^{21} cm^{-3} were realized by doping the films with Sn.[20]

For the electrical and thermoelectric measurements the wafers were cleaved into approximately 4×6 mm^2 rectangular chips. Ohmic contacts were prepared by pressing small indium pieces on the bare surface of the samples, and the ohmic contact formation was facilitated by the existing surface electron accumulation layer.[21] The Hall sheet electron concentration n_{2D} and the electrical conductivity σ were measured employing Hall effect and conductivity measurements, respectively, in van der Pauw geometry,[22] with contacts in the corners.[23] The Hall volume electron concentration n_H was determined by dividing n_{2D} by the total thickness of the In_2O_3 layer. The highest-mobility, lowest-electron-concentration sample, coinciding with sample S3 in Ref. 5, was measured to higher temperatures to analyze the phonon scattering, whose relative impact on mobility is maximized at these conditions.

The large thickness of all our films ensured that the electron transport properties were dominated by the bulk of the film rather than a possible interfacial carrier system, and the contribution of the surface electron accumulation layer to the transport was negligible.[5,21]

B. Setup to measure the Seebeck coefficient

Figure 1 schematically shows the experimental setup employed for measuring the Seebeck coefficient in air at RT. The approximately 4×6 mm^2 large sample was placed between the Peltier elements and temperature differences ΔT up to 15 K were applied. Ohmic contacts were confirmed by the linearity of the current-voltage curves measured between the contacts. Heat conduction paste (type KP92) formed a thermally conducting bridge but provided electrical isolation between the thermocouples and the sample surface. The thermoelectric potential V_{TH}, on the order of a few mV, was measured simultaneously to ΔT using high-impedance voltmeters (Keithley 4200-SCS, SMU cards). The negative ratio of the thermoelectric potential and the temperature difference is defined as the Seebeck coefficient. In detail, the measured Seebeck coefficient S_{meas} is given by the difference of the Seebeck coefficient of the sample S_{sample} and that of the voltage probes S_{probe}, where $S_{probe(W)} = 0.9\ \mu$V/K is negligible compared to $|S_{sample(In_2O_3)}| > 10\ \mu$V/K. To remove the influence of any voltage offsets we used the differential

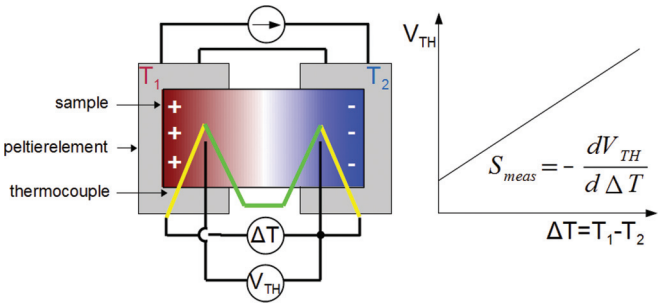

FIG. 1. (Color online) Schematics of the experimental setup to measure the Seebeck coefficient S_{meas}. Two Peltier elements produce a temperature difference $\Delta T = T_1 - T_2$ within the sample by heating one side while cooling the opposite side. The temperature difference is measured by two thermocouples, one at each side of the sample in close vicinity to the electrical contacts. In open circuit conditions the thermoelectric potential V_{TH} is measured at these contacts with a voltmeter.

method in steady-state conditions and determined the Seebeck coefficient as[24]

$$S_{\text{meas}} \approx S_{\text{sample}} = -\frac{dV_{\text{TH}}}{d\Delta T}. \quad (1)$$

III. RESULTS

A. Measured Seebeck coefficient, $S(n_H) \rightarrow n_H(S)$

Figure 2 shows a semilogarithmic plot of the measured RT Seebeck coefficient of In_2O_3 as a function of Hall volume

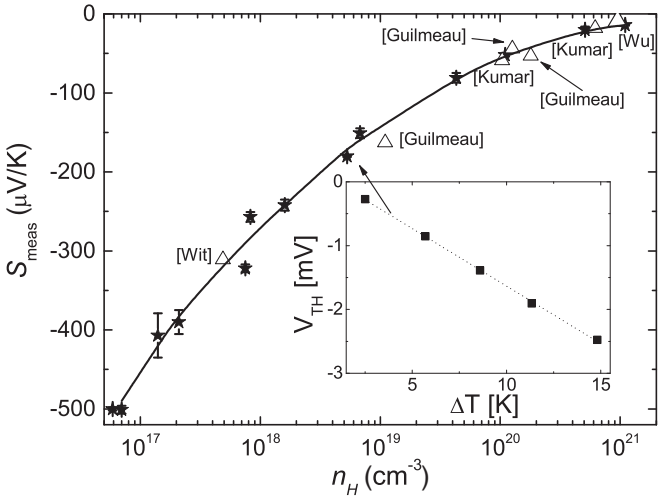

FIG. 2. Measured Seebeck coefficient S_{meas} (solid stars) as a function of the Hall volume electron concentration n_H of In_2O_3. The solid line represents our suggested empirical relation of Seebeck coefficient and Hall volume electron concentration. The error bars represent the reproducibility of the measurements. Results from literature are included (open triangles): Guilmeau *et al.*,[15] de Wit, Van der Bom, and de Groot,[10] Kumar *et al.*,[11] and Wu *et al.*[12] Corresponding mobility data for our own samples and those by Guilmeau *et al.* are shown in Fig. 3. The inset shows the measured thermoelectric potential V_{TH} as a function of the temperature difference ΔT for one sample with a best-fit straight line. The negative slope of this line is the Seebeck coefficient (marked by the arrow).

electron concentration. The negative sign of the Seebeck coefficient indicates n-type conductivity and the magnitude of S_{meas} decreases with increasing volume electron concentration. The Seebeck coefficient ranges from $\sim -500\ \mu$V/K at $n_H = 7 \times 10^{16}$ cm^{-3} to $\sim -10\ \mu$V/K at 10^{21} cm^{-3}.

As a first immediate application, the empirical $S(n_H)$ relation (solid line in Fig. 2) can be used as a calibration curve to estimate the Hall volume electron concentration in other In_2O_3 samples based on their measured Seebeck coefficient, i.e., as $n_H(S)$. The low relative deviation of the measured Seebeck coefficients (data points, also from other groups and sample types) from this empirical calibration curve would translate into a factor of 2 uncertainty for n_H. Comparison to the corresponding relative deviation in mobility (cf. Fig. 3) shows that the Seebeck coefficient is much less sensitive to the detailed scattering mechanisms than the mobility.

B. Hall mobility

The Hall mobility as function of Hall electron concentration is shown in Fig. 3. The general trend of decreasing mobility with increasing electron concentration can be observed, and is typically related to the increasing impact of ionized impurity scattering due to increasing donor concentration. Interestingly, a local peak or plateau of the mobility is observed around $n_H = 10^{20}$ cm^{-3}, which will be qualitatively explained by our mobility modeling. The large spread of mobilities, e.g., around $n_H = 10^{19}$ and 2×10^{20} cm^{-3}, indicates additional scattering in the lower-mobility samples, e.g., due to compensating acceptors, dislocations, or grain boundaries, and demonstrates that the electron mobility is a very sensitive probe to imperfections in the crystal. For example, the polycrystalline bulk ceramic samples by Guilmeau *et al.* but also single-crystalline thin film samples by Ohta *et al.* show comparably

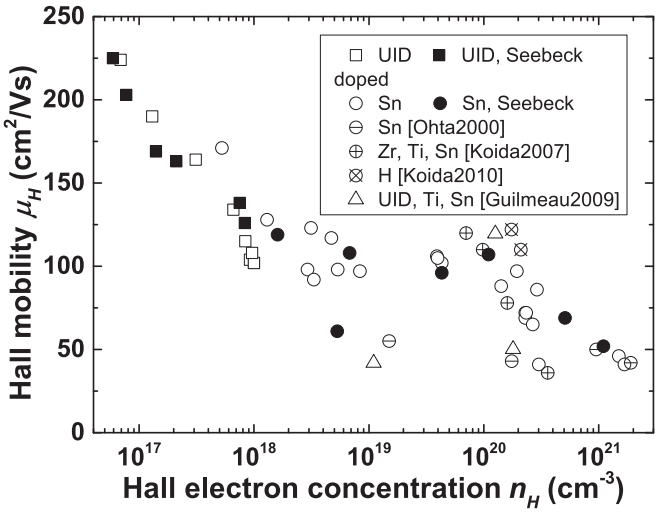

FIG. 3. Measured Hall mobilities μ_H as a function of the Hall volume electron concentration n_H of In_2O_3. UID (squares) and Sn-doped (circles) samples are marked separately. Results on doped In_2O_3 from literature are included (Ohta *et al.*,[25] Koida and Kondo,[26] Koida *et al.*,[27] and Guilmeau *et al.*).[15] The corresponding Seebeck data can be found in Fig. 2 for our samples (marked here by solid symbols) and for those by Guilmeau *et al.* (open triangles).

TABLE I. Parameters used for the numerical modeling. *Within this study we have derived T_D and N_{OPML} by modeling the high-temperature mobility, and m^* by careful comparison of electron concentration and Seebeck coefficient taking into account the modeled Hall scattering factor. #The charge of ionized impurities has been considered 2 for oxygen vacancies or 1 for Sn donors.

Parameter (physical unit)	Value
Debye temperature Θ_D (K)	700*
Effective electron mass m^* (m_e)	0.30* (0.22)[31]
Longitudinal optical phonon modes N_{OPML}	1.33 (2.15)*
Charge of ionized impurity Z (e)	1 and 2#
Band gap (eV)[32]	2.9
Relative permittivity at high frq. $\epsilon_{r,\infty}$ (ϵ_0)[33]	4.0
Static dielectric constant $\epsilon_{r,0}$ (ϵ_0)[33]	9.0
Number of atoms per cubic unit cell N[34]	80
Lattice constant a (nm)[34]	1.0118
Density ρ (kg/m^3)[34]	7.12×10^3
Longitudinal elastic constant c_l (Pa)[35]	3.0×10^{11}
Sound velocity $v_S = \sqrt{c_l/\rho}$ (m/s)[36]	6.4×10^3
Acoustic deformation potential D_a (eV)[35]	−4.31

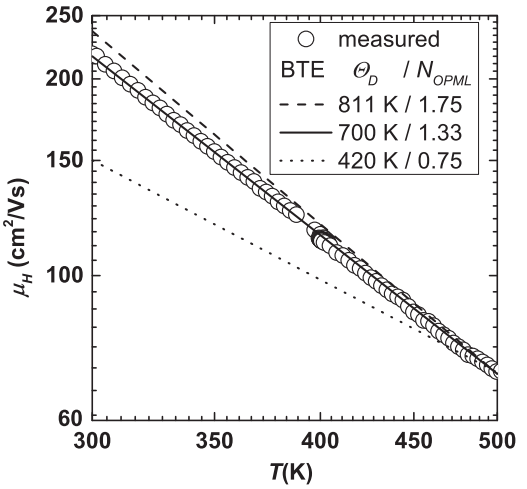

FIG. 4. Temperature dependent Hall mobility of a high mobility UID sample and mobility fit. Besides POP scattering, the fit takes into account IIS, ADP scattering, and the Hall scattering factor. The parameter set for POP scattering was varied to fit the mobility at $T = 500$ K.

low mobilities around $n_H = 10^{19}$ and 2×10^{20} cm^{-3}. On the other hand, another ceramics sample by Guilmeau *et al.* at $n_H \approx 1.5 \times 10^{20}$ cm^{-3} shows one of the highest reported mobilities.

IV. MODELING AND DISCUSSION

A. Numerical solution to the Boltzmann transport equation

The mobility and Seebeck coefficient is modeled by solving the BTE using an extension of Rode's iterative method.[28] This approach treats the full BTE—as opposed to the truncated linear form[29] frequently used in the literature—which enhances its validity at degenerate doping levels. The theoretical finding, that Sn doping does not significantly influence the band structure due to donor bands,[30] encourages us to provide the numerical solution up to very high Sn concentrations (up to 10^{21} cm^{-3}). Our approach does not rely on the relaxation time approximation, thereby describing optical-mode phonon in-scattering, and includes the nonparabolicity of the conduction band of In_2O_3 as well as Pauli's exclusion principle. Details on the implementation are given in Ref. 19.

The relevant material parameters for the modeling, shown in Table I, were taken from literature or were extracted in this work, which makes the transport modeling an iterative, self-consistent procedure: for example, modeling of the electron mobility allowed us to extract the Hall scattering factor and Seebeck scattering parameter. These enter the modeling of the Seebeck coefficient, which together with the Hall data was used to extract the effective electron mass, which entered the mobility modeling.

B. Mott criterion, degeneracy

The Mott criterion[37] $n_{nd} < (0.26 a_B m^*/m_e/\epsilon_r)^3 < n_d$ (with hydrogen Bohr radius $a_B = 0.053$ nm, relative dielectric permittivity at low frequency of In_2O_3 $\epsilon_r = 9$,[33] and m^*) defines the Mott transition from nondegenerate (indicated by subscript "nd") to degenerate (indicated by subscript "d") electron concentrations. For $m^* = 0.30 m_e$, extracted in this study, we find the Mott transition at $n_{\mathrm{Mott}} = 5.5 \times 10^{18}$ cm^{-3}.

C. Scattering mechanisms and mobility

For simplification and due to a lack of independent data on dislocations, compensating acceptors, or grain sizes for the samples with lower mobility, the modeling will be limited to the dominant intrinsic scattering mechanisms, i.e., scattering by phonons and by the ionized donors, similar to Ref. 38. Indeed, we have already shown that our nondegenerate, high-quality samples are clearly dominated by phonon scattering and that the donors are fairly shallow.[5] Therefore, almost all donors are ionized, and this trend will even increase towards higher doping levels (where impurity scattering becomes more important) as the samples turn degenerate. Because the number of neutral donors is negligible in this case, we can neglect neutral impurity scattering. Electron-electron scattering, as suggested to be important in Ref. 15, can also be neglected as it does not change the total electron momentum and thus not the mobility.

1. Ionized impurity scattering and charge of impurity

We have strong evidence for doubly charged bulk oxygen vacancies[6] to act as shallow donors in our UID In_2O_3 samples.[5,39] Sn donors, in contrast, are only singly charged in the In_2O_3 lattice. Ionized impurity scattering (IIS) for both cases is modeled. For a given electron concentration, fully ionized donors, and the absence of compensation, the mobility due to IIS from doubly charged donors is exactly half that due to IIS from singly charged donors.[6]

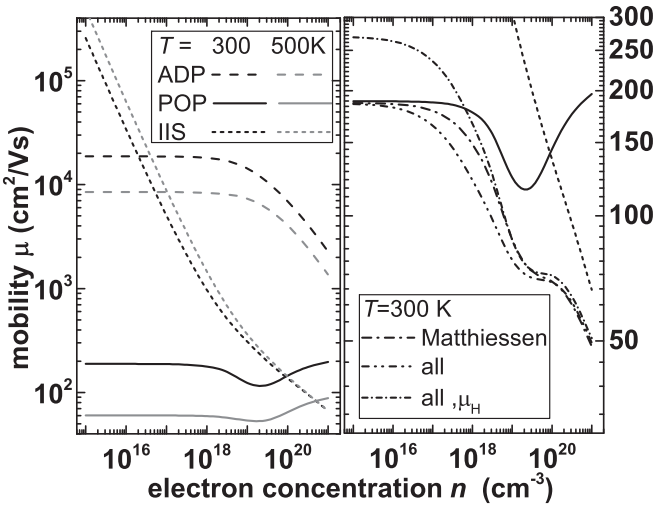

FIG. 5. Modeled RT (300 K) mobility as function of electron concentration for different scattering mechanisms: ADP = acoustic deformation potential; POP = polar optical phonon; IIS = ionized impurity scattering. (As indicator for the temperature dependence and for comparison with Fig. 4, the modeled mobilities at 500 K are also shown). Left: overview for individual scattering mechanisms. Right: modeled individual mobility due to POP and IIS scattering, approximated total mobility using Matthiessen's rule and the individual mobilities, modeled total mobility, and modeled total Hall mobility (taking into account the modeled Hall scattering factor of Fig. 6).

2. *Phonon scattering and effective Debye temperature of polar optical phonons*

Due to the polar nature of the In_2O_3 crystal with partly polar bonds between In and O atoms, optical phonon scattering and acoustic phonon scattering limit the electron mobility. The acoustic phonon scattering is purely acoustic deformation potential (ADP) scattering as piezoelectric scattering can be ruled out because the bcc bixbiyte crystal structure of In_2O_3[34] is centrosymmetric. The mainly s-like symmetry of the In_2O_3 conduction band (made up of In 5s orbitals)[31] leads to vanishing scattering due to optical deformation potential,[40] which means that the optical phonon scattering is purely due to longitudinal polar optical phonons (POP).[36] The fact that ADP scattering is less important than POP scattering in polar semiconductors such as In_2O_3 can be seen with the modeled mobilities in Fig. 5, and is related to the generally larger coupling constant for polar interactions than for a deformation potential.[40] The physical quantities to model the ADP scattering: density ρ, velocity of sound v_s, and acoustic deformation potential D_a (given in Table I), have been extracted from the available literature. Even though some of these parameters are approximate only, they do not drastically change the magnitude of the ADP scattering rate.

POP scattering is characterized by the longitudinal optical phonon energy, parametrized as Debye temperature Θ_D, and the number of longitudinal optical phonon modes N_{OPML}. The large number of 80 atoms in the cubic bixbyite In_2O_3 unit cell[34] results in a complex phonon spectrum with many longitudinal optical phonon modes of different phonon energy.[41] With this spectrum Θ_D cannot be assigned to a single phonon energy, and setting N_{OPML} equal to the high number of phonon modes results in unrealistically low modeled mobilities. Therefore, only an effective Θ_D and N_{OPML} can describe the POP scattering in In_2O_3. Published Debye temperatures of In_2O_3 range from 420 K[42] to 650–811 K (corresponding to phonon energies 56–70 meV).[41] A simple approximation,[43] $\Theta_D = \frac{h v_S}{2\pi k_B}\sqrt[3]{\frac{6\pi^2 N}{V}}$, based on number density of atoms N/V and speed of sound v_S, given Table I, also results in a Debye temperature of $\Theta_D = 811$ K.

To find suitable effective Θ_D and N_{OPML} we are fitting our modeled mobility (including IIS and ADP scattering) to the temperature dependent mobility data above RT of a sample with high mobility and low donor concentration (sample S3 from Ref. 5). This choice of sample and temperature ensures a maximized impact of phonon scattering and a minimized impact of all other scattering mechanisms on the mobility. The comparison shown in Fig. 4 was performed for an electron effective mass $m^* = 0.30m_e$ but the fit was repeated for $m^* = 0.22m_e$, which will be discussed later. We note that, in this double-logarithmic plot, Θ_D mainly determines the slope, whereas m^* and N_{OPML} result mainly in a vertical displacement of the modeled curve. Therefore, Θ_D is rather independent of the chosen m^* and N_{OPML} can be adjusted to the used m^*: an effective Debye temperature of $\Theta_D = 700$ K with effective number of longitudinal optical phonon modes $N_{\mathrm{OPML}} = 1.33(2.15)$ for $m^* = 0.30(0.22)m_e$ best describes our experimental data, and is our recommended parameter set for modeling the POP scattering.

3. *Comparison of scattering mechanisms, maximum mobility*

Figure 5(left) gives an overview of our modeled RT mobilities due to different scattering mechanisms as a function of electron concentration n. It clearly demonstrates a dominant POP scattering at low electron concentrations and negligible ADP scattering at all electron concentrations. This finding contrasts the early interpretation of Ref. 2 that assigns acoustic phonon scattering and ionized impurity scattering as main scattering mechanisms. The mobility due to POP scattering is fairly constant at low n, and our model predicts a maximum RT mobility of 190 $\mathrm{cm^2/V\,s}$ towards vanishing n and related donor concentration N_D. The mobility due to POP scattering decreases from $n = 2 \times 10^{18}$ and 2×10^{19} $\mathrm{cm^{-3}}$, indicating the onset of optical phonon emission as the kinetic electron energy approaches the longitudinal optical phonon energy. The increasing POP mobility to higher electron concentrations is due to increasing screening of the optical phonons.[44]

IIS, modeled for singly charged and fully ionized donors, dominates POP scattering at n ($n = N_D$) above 10^{20} $\mathrm{cm^{-3}}$. Figure 5(right) demonstrates that even at these high electron concentrations POP scattering has a non-negligible influence on the total mobility and can explain the discrepancy of measured and modeled mobility in Refs. 6 and 7, which disregarded phonon scattering.

4. *Hall scattering factor, maximum Hall mobility*

The Hall scattering factor r_H is an often neglected quantity, which relates the drift mobility μ and carrier concentration n to the corresponding quantities Hall mobility μ_H and Hall concentration n_H, obtained from Hall measurements, as

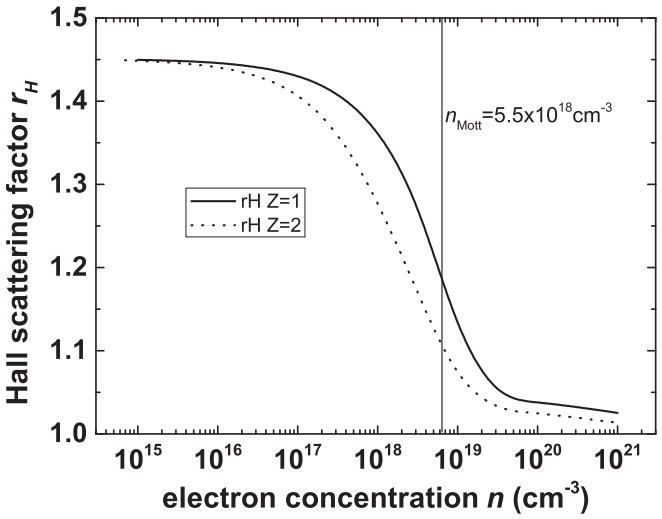

FIG. 6. Modeled Hall scattering factor r_H at RT as a function of electron concentration for singly charged ($Z = 1$) and doubly charged ($Z = 2$) donors.

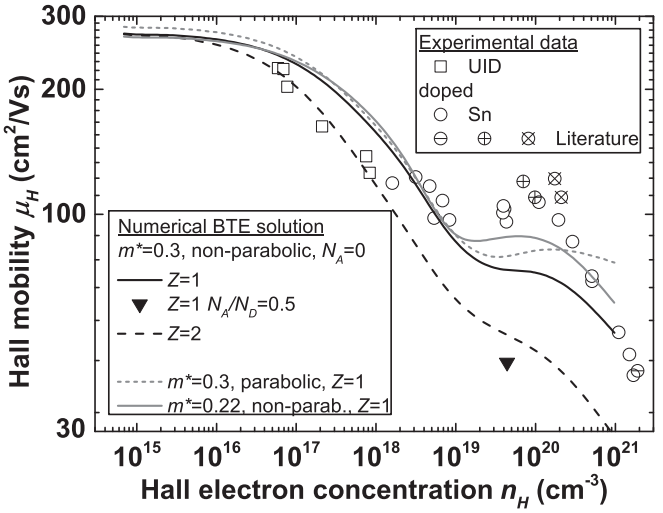

FIG. 7. Comparison of measured (symbols) and modeled (lines) RT Hall mobility as function of Hall electron concentration. Modeling was performed for a parabolic or nonparabolic conduction band structure with different effective masses m^*, for singly ($Z = 1$) and doubly ($Z = 2$) ionized donors. Compensation was assumed to be absent (acceptor concentration $N_A = 0$). (In correspondence to a modeled Seebeck coefficient in Fig. 9 one data point (solid triangle) was modeled for compensation with $N_A/N_D = 0.5$.) The parameters from Table I were used for the modeling. Nonparabolic band structures were implemented by using a simple $\mathbf{k} \cdot \mathbf{p}$ model as described in Eq. (1) of Ref. 31.

$\mu = \mu_H/r_H$ and $n = r_H n_H$. It can assume values $1 \leqslant r_H \leqslant 2$, is close to unity at degenerate carrier concentrations (which is why it could be neglected in most published literature on In_2O_3), and its deviation from unity at nondegenerate carrier concentrations depends on the scattering mechanisms. The Hall scattering factor extracted from our mobility modeling is shown in Fig. 6 and is used to convert measured data (n_H, μ_H) to the quantities (n, μ) used in the modeling. At nondegenerate electron concentrations, well below the Mott density, $r_H \approx 1.45$. At the Mott electron concentration $r_H \approx 1.2$, and becomes close to unity well above this concentration. The discrepancy between modeled Hall mobility and modeled mobility can be seen by comparing the mobility curves "all" and "all, μ_H" in Fig. 5(right). Consequently, our model predicts a maximum RT Hall mobility (at negligible ionized impurity concentration) of 270 cm^2/V s, which is close to our empirically suggested value of 274 cm^2/V s in Ref. 5.

5. *Comparison of measured and modeled mobility*

For the comparison of modeled and measured Hall mobility, shown in Fig. 7, we consider only the highest experimental values (our own and published by others as indicated) for each electron concentration, as these are less likely influenced by additional scattering mechanisms (dislocation, compensation, and grain boundaries). As indicated, the mobility modeling was performed for parabolic and nonparabolic conduction bands with different effective masses. Effective masses of $0.22m_e$ and $0.3m_e$ were chosen to represent two distinctly different but widely used values (see Table II). Simultaneous scattering by polar optical phonons, acoustic deformation potential, and ionized impurities as shown in Fig. 5 was considered. We assumed uncompensated, fully ionized donors with charge of 2 (ionized oxygen vacancies) or 1 (ionized Sn-donor) to act as ionized impurities.

For Hall electron concentrations up to 10^{19} cm^{-3} the modeled mobility is relatively insensitive to the chosen band structures, and reproduces the experimental values very well. The close fit for UID films to the model with a donor charge of $Z = 2$ and that of the Sn-doped films to the model with $Z = 1$ strongly supports our assumption of doubly charged oxygen vacancies to act as UID donors. (See Fig. 7.)

A plateau or local maximum of the experimental mobility is observable between $n_H = 10^{19}$ and 2×10^{20} cm^{-3}, which is qualitatively reproduced by the modeled mobility. Comparison to Fig. 5(right) clarifies that this plateau arises from a coinciding decreasing mobility due to IIS and increasing mobility due to POP scattering with increasing electron concentration. The model, however, clearly underestimates the mobility irrespective of the assumed band structure, which could be related to an underestimated screening of the optical phonons,[45] as for example described by Ehrenreich.[46] The fit is closer for a band structure with $m^* = 0.22m_e$, even though our Seebeck and Hall data clearly indicates $m^* = 0.3m_e$. We speculate that this contradiction could be resolved by a modified screening approximation for optical phonons at high electron concentrations.

At $n_H > 2 \times 10^{20}$ cm^{-3}, the Hall mobility decreases again due to the predominant IIS [cf. Fig. 5(right)]. It is clearly better described by a nonparabolic band structure, which is consistent with the onset of the nonparabolicity at high electron concentrations.

D. Seebeck coefficient

Two approaches are used to model the Seebeck coefficient: the first approach employs commonly used, simplified equations and the second approach is based on the numerical solution of the BTE described above. All parameters which

are used for the modeling are listed with corresponding value for In_2O_3 in Table I.

1. Simplified equations

There are two simplified, commonly used equations[36] to calculate Seebeck coefficients as a function of volume electron concentration n, effective electron mass m^*, and Seebeck scattering parameter r which is related to the scattering mechanisms within the sample. The first of these equations is valid for nondegenerate volume electron concentrations, while the second one is valid for degenerate volume electron concentrations:

$$S_{nd}(m^*,n,r) = -\frac{k_B}{e}\left(r+\frac{5}{2}-\eta\right),$$
$$S_d(m^*,n,r) = -\frac{k_B}{e}\left(r+\frac{3}{2}\right)\frac{\pi^2}{3}\frac{1}{\eta}. \quad (2)$$

On the right hand side, $\eta(n,m^*,T) = [E_F(m^*,n,T) - E_C]/[k_BT]$ is the reduced electron chemical potential. E_F is the Fermi energy, E_C the conduction band minimum energy, and k_BT the thermal energy with Boltzmann constant k_B. Both equations are restricted to the relaxation time approximation and to a parabolic conduction band. Furthermore, Eqs. (2) are based on the assumption that the relaxation time τ follows a simple power law dependence on the electron kinetic energy E^r with the energy exponent r being the Seebeck scattering parameter. This power law dependence is appropriate for elastic scattering processes such as ionized impurity scattering for which $r = 1.5$,[47] but it fails for inelastic scattering processes such as polar optical phonon in-scattering where τ is not defined and r is not a constant. For the latter case, Ehrenreich determined an effective Seebeck scattering parameter r as a function of Θ_D/T.[48]

Based on our mobility modeling we determine the appropriate r for evaluating S with Eqs. (2): we found acoustical phonon scattering to be completely negligible, polar optical phonon scattering to dominate the mobility for volume electron concentrations up to 10^{20} cm^{-3}, and scattering at ionized impurities to dominate above this concentration. Therefore, we obtain a Seebeck scattering parameter $r = -0.55 \pm 0.01$ for polar optical phonon scattering from the results of Ehrenreich *et al.*[48] and $\Theta_D = 700$ K extracted from our mobility fit. The error bar of r covers Debye temperatures from 650 to 811 K, which correspond to results obtained from infrared lattice vibrations of In_2O_3.[41,49] The modeled Seebeck coefficient based on the numerical solution to the BTE is also quite similar using the two different values for Θ_D.

The reduced electron chemical potential η depends on the effective electron mass m^*, the volume electron concentration n, and the temperature T. For this dependence we used an analytical expression, suggested by Nilsson *et al.*,[50] which is valid for the full range of volume electron concentrations (nondegenerate and degenerate):

$$\eta = \frac{\ln\frac{n}{N_C}}{1-\left(\frac{n}{N_C}\right)^2} + v\left(1-\frac{1}{1+(0.24+1.08v)^2}\right), \quad (3)$$

$$v = \left(\frac{3\sqrt{\pi}\frac{n}{N_C}}{4}\right)^{\frac{2}{3}}, \quad (4)$$

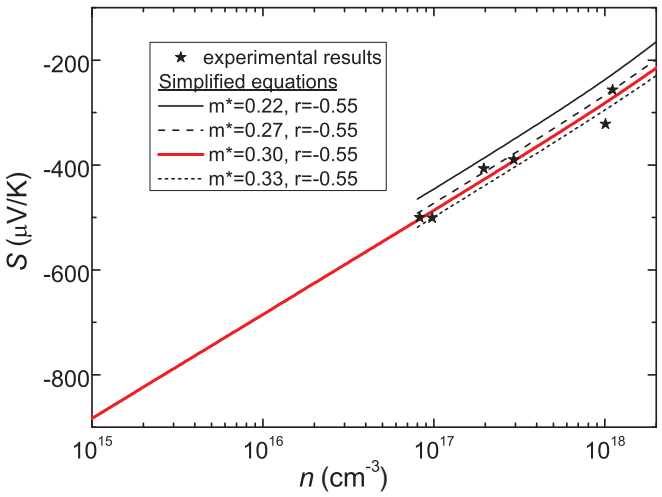

FIG. 8. (Color online) Measured Seebeck coefficient (black stars) as a function of the nondegenerate volume electron concentrations. The lines represent modeled Seebeck coefficients using the simplified equation for the nondegenerate case. Different effective masses are considered as indicated. The long, red line represents the best fit and serves as theoretically expected $S(n)$ relation for smaller electron concentrations.

with the effective density of conduction band states N_C given by

$$N_C = 2\left(\frac{2\pi m^* k_B T}{h^2}\right)^{\frac{3}{2}}. \quad (5)$$

2. Effective electron mass

In the nondegenerate regime ($n < 10^{18}$ cm^{-3}) the high mobility (and its temperature dependence) in our samples indicated dominant optical phonon scattering at RT with known Seebeck scattering parameter r. This knowledge of r allowed us to estimate m^* from the measured Seebeck coefficients S and electron concentrations n. The electron concentration n was calculated from the measured Hall concentration n_H and the modeled Hall scattering factor r_H as discussed above. The effective mass is extracted by fitting our data to the simplified Eq. (2) together with Eqs. (3)–(5) as shown in Fig. 8. The extracted effective electron mass is $m^* = (0.30 \pm 0.03)m_e$. (We note that an effective electron mass of $m^* = 0.24m_e$ would be extracted if the Hall scattering factor was not taken into account.)

Extending the solid, red fit line towards smaller n immediately yields a theoretical relation $S(n)$ for smaller electron concentrations than investigated in this paper.

Quite diverse values have been reported in the literature for $m^*$of In_2O_3. They have been obtained by different methods as traditional experiments such as cyclotron resonance are not easily applicable to transparent conducting oxides due to their low mobility.[47] Table II shows a survey of literature data on the effective mass values for In_2O_3 with corresponding methods and references. Two other groups, which extracted the effective mass by the same methods as ours, obtained markedly different results: Ref. 10 determined a lower $m^* = 0.14m_e$ based on above RT Hall and Seebeck measurement of one

TABLE II. Survey of data on the effective mass values for UID In_2O_3. Apart from the method used in this study ("Hall + Seebeck"), spectroscopic ellipsometry ("Ellipsometry"), angular resolved photo electron spectroscopy of the conduction band ("ARPES"), and density functional theory ("DFT") were used in the given references. To reflect the density of states effective mass, we averaged the "ARPES" results of Ref. 51 for the ΓP and ΓN directions, $m^*_{\Gamma P} = (0.18 \pm 0.02)m_e$ and $m^*_{\Gamma N} = (0.24 \pm 0.02)m_e$, respectively.

m^* (m_e)	Method	Ref.
0.14	Hall + Seebeck	10
0.55	Hall + Seebeck	2
0.30	Ellipsometry	52
0.22	DFT calculation	31
0.21 ± 0.03	ARPES	51
0.22	ARPES	53
0.30 ± 0.03	Hall + Seebeck	This work

sample at essentially the same volume electron concentration and scattering exponent r as used by us. That sample was polycrystalline and no information on the mobility was given. Reference 2 mentioned a significantly higher effective mass of $m^* = 0.55m_e$, but did not give any details on their modeling. The effective mass value extracted in our work is consistent with that found by ellipsometry.[52] Results from angular-resolved photo electron spectroscopy (ARPES)[51,53] are systematically smaller than this value but consistent with the DFT calculated value from Ref. 31. A possible explanation of the discrepancy of the experimental values for m^* by ARPES and our method or ellipsometry might be a different band structure at the In_2O_3 surface (probed by ARPES) than in the bulk (probed by ellipsometry or our method). A comparison of the numerically modeled Seebeck coefficients in Fig. 9 demonstrates that at all electron concentrations $m^* = 0.30m_e$ better fits our experimental Seebeck results than $m^* = 0.22m_e$. Consequently, we propose a value of $m^* = (0.30 \pm 0.03)m_e$.

3. Comparison of measured and modeled Seebeck coefficient

Figure 9 shows the modeled Seebeck coefficient of In_2O_3 as a function of the volume electron concentration using the two approaches discussed above. The charge of the ionized impurities is $Z = 1$ for the samples doped with tin donors. The measured results (with n_H corrected by the modeled r_H to represent the true electron concentration) are also shown for comparison.

The simplified equations were evaluated for pure optical phonon scattering ($r = -0.55$) and for pure ionized impurity scattering ($r = 1.5$) separately. At electron concentrations lower than 2×10^{18} cm^{-3} the simplified model for the nondegenerate regime [S_{nd} in Eqs. (2)] and optical phonon scattering describes the measured data well, which is in agreement with our mobility evaluations here and in Ref. 5. At concentrations greater than about 10^{19} cm^{-3} the experimental results are in between the theoretical curves of the degenerate regime [S_d in Eqs. (2)] for optical phonon scattering and ionized impurity scattering. With increasing doping concentration the measured Seebeck coefficient approaches the modeled one

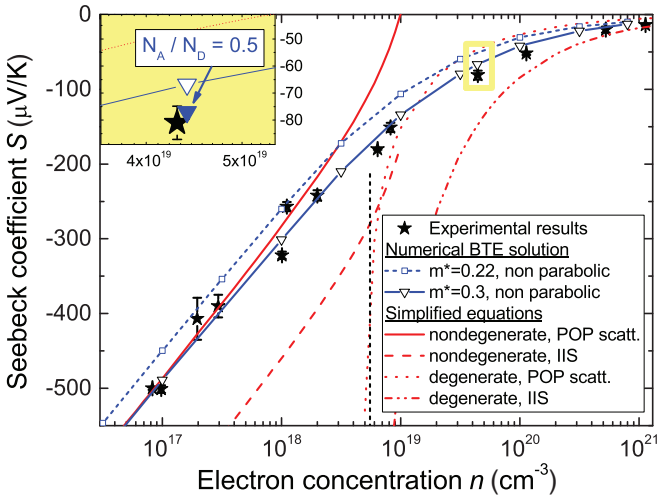

FIG. 9. (Color online) Lines show the modeled Seebeck coefficients as a function of the volume electron concentration for In_2O_3 at RT. The solid blue line with open triangles corresponds to the numerical solution of the BTE, taking into account POP scattering and IIS with fully ionized donors ($n = N_D$) and no compensating acceptors ($N_A = 0$). The results of simplified approximations [Eqs. (2)] for nondegenerate and degenerate volume electron concentrations are also shown (red lines), with $r = 1.5$ for IIS and $r = -0.55$ for POP scattering. The vertical line denotes the Mott transition with the nondegenerate regime to the left and the degenerate regime to the right. Solid black stars correspond to measured Seebeck coefficients (cf. Fig. 2). The inset (top left) shows an additional numerical solution of the BTE (solid blue triangle) with assumed compensation.

for ionized impurity scattering. This behavior reflects the increasing contribution of ionized impurity scattering, which is in agreement with our mobility evaluations. For electron concentrations between 2×10^{18} and 10^{19} cm^{-3}, i.e., around the Mott transition at $n_{\text{Mott}} = 5.5 \times 10^{18}$ cm^{-3}, neither S_{nd} nor S_d describes the measured data well. Hence the simplified equations (2) are only valid well within the nondegenerate and degenerate regime, respectively, but none of them is valid around the Mott transition between both regimes.

Similar to the mobility, we find an excellent agreement of the Seebeck coefficient based on the numerical solution of the BTE and the measured results at volume electron concentrations up to 10^{19} cm^{-3} and including the Mott transition. For electron concentrations around 10^{20} cm^{-3}, however, the magnitude of the measured Seebeck coefficient is systematically larger than that of the modeled one. Increased ionized impurity scattering due to strong compensation (with a ratio of acceptor to donor concentration $N_A/N_D = 0.5$) as shown in the inset of Fig. 9 could explain the difference but would result in a drastic discrepancy of the corresponding modeled mobility from the measured one (cf. triangle symbol in Fig. 7). Strong compensation is therefore unlikely and a more likely reason is the underestimated mobility due to POP scattering around $n = 10^{20}$ cm^{-3}, that we already found with the mobility modeling: a stronger screened POP scattering would also increase the relative contribution of the IIS, which should move the modeled Seebeck coefficient towards the simplified case of only IIS (red dash-dot-dot line in Fig. 9), i.e., to a higher magnitude.

V. SUMMARY

We presented a systematic study of room-temperature electron transport and electrothermal transport in In_2O_3 as function of electron concentration n. The high quality and purity of our single-crystalline films allowed us to investigate previously unexplored, nondegenerate volume electron concentrations as low as 10^{17} cm^{-3} in unintentionally doped films. Electron concentrations up to 10^{21} cm^{-3} were realized by Sn doping. Room temperature Hall measurements and measurements of the Seebeck coefficient S in our films were performed for electron concentrations from 10^{17} to 10^{21} cm^{-3}. An immediate, practical application of the measured relation $S(n)$ is its use to estimate the volume electron concentration in other In_2O_3 samples based on their measured Seebeck coefficient. This estimated volume electron concentration can help clarify if a sheet concentration measured by the Hall method represents a thick bulk or a true sheet carrier system. An additional temperature dependent Hall measurement of a high-mobility, low-electron-concentration sample above room temperature provided data to understand phonon scattering in In_2O_3.

Consistently fitting the electron mobility and Seebeck coefficient as function of electron concentration (or temperature) to a numerical solution of the Boltzmann transport equation allowed us to determine the main scattering mechanisms, their parameters, and the effective electron mass as follows.

(i) Phonon scattering and ionized impurity scattering sufficiently well describe the measured data for samples with the highest mobility (which are less influenced by structural defects or compensating impurities) at each electron concentration.

(ii) Polar optical phonon scattering, best described by a Debye temperature of $\Theta_D = 700$ K and $N_{\mathrm{OPML}} = 1.33$ phonon modes, is the dominant phonon scattering mechanism which limits the room-temperature drift mobility 190 cm^2/V s. Acoustic deformation potential scattering is negligible.

(iii) Ionized impurity scattering with doubly ionized donors best describes the unintentionally doped samples, whereas singly ionized donors best describe Sn-doped samples, which supports our assumption of oxygen vacancies to act as shallow donors in the unintentionally doped samples.

(iv) The Hall scattering factor r_H, which relates Hall mobility and concentration to drift mobility and electron concentration, has been extracted, It is non-negligible (>1.1) below $n = 10^{19}$ cm^{-3}. The maximum room-temperature Hall mobility, limited by phonon scattering, is 270 cm^2/V s.

(v) An effective electron mass of $m^* = 0.30 \pm 0.03$ times the free electron mass best describes the measured Seebeck coefficient.

The numerical solution of the Boltzmann transport equation provides excellent agreement to the measured data up to electron concentrations of 10^{19} cm^{-3}, and qualitatively explains the plateau or local maximum of the electron mobility around electron concentrations of 10^{20} cm^{-3} by the combined effect of increasing scattering due to ionized impurities and decreasing scattering due to increasing screening of optical phonons. A systematic deviation of experimental data to higher mobilities and higher magnitude Seebeck coefficient at these concentrations would be consistent with a quantitatively underestimated screening of polar optical phonons.

The In_2O_3 Seebeck coefficient was additionally compared to the widely used, simplified equations for either nondegenerate or degenerate volume electron concentrations. A simplified equation together with the Seebeck scattering parameter $r = -0.55$, corresponding to the Debye temperature for POP scattering in In_2O_3, describes our nondegenerate samples very well, and was used to provide a theoretical estimate of the Seebeck coefficient for lower electron concentrations than experimentally realized in this work. At degenerate electron concentrations, the simplified equation using $r = -0.55$ (POP scattering) and $r = 1.5$ (ionized impurity scattering) describes the upper and lower bound of the Seebeck coefficient well. The simplified equations proved invalid around the Mott transition at $n_{\mathrm{Mott}} \approx 5.5 \times 10^{18}$ cm^{-3} from nondegenerate to degenerate electron concentrations, whereas the numerical solution of the Boltzmann transport equation described this region very well.

ACKNOWLEDGMENTS

We would like to thank K.-J. Friedland for critically reading the manuscript and Tom Mates for support with the SIMS measurements. Additional theoretical insights by Aron Walsh, Péter Ágoston, and Jasprit Singh are gratefully acknowledged. This work was supported in part by the National Science Foundation NSF MRSEC and MWN Programs under Awards No. DMR05-20415 and No. DMR09-09203. A portion of this work was done in the UCSB nanofabrication facility, part of the NSF-funded NNIN network. O.B. was supported by a grant from the AFOSR Award No. FA9550-08-1-0461. We wish also to thank John E. Bowers (ECE Department, UCSB) for helpful discussions. A.T.R. acknowledges support by the Center for Energy Efficient Materials, an Energy Frontier Research Center funded by the US Dept. of Energy, Office of Basic Energy Sciences, under Award No. DE-SC0001009.

*Also at Materials Department, University of California, Santa Barbara, CA 93106, USA; bierwagen@pdi-berlin.de

[1]Z. Galazka, K. Irmscher, M. Pietsch, T. Schulz, R. Uecker, D. Klimm, and R. Fornari, CrystEngComm. **15**, 2220 (2013).

[2]R. L. Weiher, J. Appl. Phys. **33**, 2834 (1962).

[3]O. Bierwagen, M. E. White, M. Y. Tsai, and J. S. Speck, Appl. Phys. Lett. **95**, 262105 (2009).

[4]O. Bierwagen and J. S. Speck, J. Appl. Phys. **107**, 113519 (2010).

[5]O. Bierwagen and J. S. Speck, Appl. Phys. Lett. **97**, 072103 (2010).

[6]R. B. H. Tahar, T. Ban, Y. Ohya, and Y. Takahashi, J. Appl. Phys. **83**, 2631 (1998).

[7]T. Koida and M. Kondo, J. Appl. Phys. **99**, 123703 (2006).

[8]O. Bierwagen, S. Choi, and J. S. Speck, Phys. Rev. B **84**, 235302 (2011).

[9]O. Bierwagen, T. Nagata, M. E. White, M. Y. Tsai, and J. S. Speck, J. Mater. Res. **27**, 2232 (2012).
[10]J. H. W. de Wit, J. Van der Bom, and J. F. de Groot, J. Solid State Chem. **25**, 101 (1978).
[11]M. Kumar, R. Chatterjee, S. Milikisiyants, A. Kanjilal, M. Voelskow, D. Grambole, K. V. Lakshmi, and J. P. Singh, Appl. Phys. Lett. **95**, 013102 (2009).
[12]C.-Y. Wu, T. V. Thanh, Y.-F. Chen, J.-K. Lee, and J.-J. Lin, J. Appl. Phys. **108**, 123708 (2010).
[13]Z. Q. Li and J. J. Lin, J. Appl. Phys. **96**, 5918 (2004).
[14]D. Bérardan, E. Guilmeau, A. Maignan, and B. Raveau, J. Appl. Phys. **104**, 064918 (2008).
[15]E. Guilmeau, D. Berardan, C. Simon, A. Maignan, B. Raveau, D. O. Ovono, and F. Delorme, J. Appl. Phys. **106**, 053715 (2009).
[16]K. Ellmer and R. Mientus, Thin Solid Films **516**, 5829 (2008).
[17]J.-H. Bahk, Z. Bian, M. Zebarjadi, J. M. O. Zide, H. Lu, D. Xu, J. P. Feser, G. Zeng, A. Majumdar, A. C. Gossard *et al*., Phys. Rev. B **81**, 235209 (2010).
[18]N. Hamada, T. Imai, and H. Funashima, J. Phys.: Condens. Matter **19**, 365221 (2007).
[19]A. T. Ramu, L. E. Cassels, N. H. Hackman, H. Lu, J. M. O. Zide, and J. E. Bowers, J. Appl. Phys. **107**, 083707 (2010).
[20]O. Bierwagen and J. S. Speck, Phys. Status Solidi A (to be published).
[21]O. Bierwagen, J. S. Speck, T. Nagata, T. Chikyow, Y. Yamashita, H. Yoshikawa, and K. Kobayashi, Appl. Phys. Lett. **98**, 172101 (2011).
[22]L. J. van der Pauw, Philips Res. Rep. **13**, 1 (1958).
[23]O. Bierwagen, T. Ive, C. G. Van de Walle, and J. S. Speck, Appl. Phys. Lett. **93**, 242108 (2008).
[24]J. Martin, T. Tritt, and C. Uher, J. Appl. Phys. **108**, 121101 (2010).
[25]H. Ohta, M. Orita, M. Hirano, H. Tanji, H. Kawazoe, and H. Hosono, Appl. Phys. Lett. **76**, 2740 (2000).
[26]T. Koida and M. Kondo, J. Appl. Phys. **101**, 063713 (2007).
[27]T. Koida, M. Kondo, K. Tsutsumi, A. Sakaguchi, M. Suzuki, and H. Fujiwara, J. Appl. Phys. **107**, 033514 (2010).
[28]D. L. Rode, Phys. Rev. B **2**, 1012 (1970).
[29]M. Lundstrom, *Fundamentals of Carrier Transport* (Cambridge University Press, Cambridge, UK, 2000).
[30]H. Odaka, Y. Shigesato, T. Murakami, and S. Iwata, Jpn. J. Appl. Phys. **40**, 3231 (2001).
[31]F. Fuchs and F. Bechstedt, Phys. Rev. B **77**, 155107 (2008).
[32]P. D. C. King, T. D. Veal, F. Fuchs, C. Y. Wang, D. J. Payne, A. Bourlange, H. Zhang, G. R. Bell, V. Cimalla, O. Ambacher *et al*., Phys. Rev. B **79**, 205211 (2009).
[33]I. Hamberg and C. G. Granqvist, J. Appl. Phys. **60**, R123 (1986).
[34]M. Marezio, Acta Crystallogr. **20**, 723 (1966).
[35]K. H. L. Zhang, V. K. Lazarov, T. D. Veal, F. E. Oropeza, C. F. McConville, R. G. Egdell, and A. Walsh, J. Phys.: Condens. Matter **23**, 334211 (2011).
[36]K. Seeger, *Semiconductor Physics*, 9th ed. (Springer, New York, 2004).
[37]N. Mott, Proc. R. Soc. A **382**, 1 (1982).
[38]D. C. Look, D. C. Reynolds, J. R. Sizelove, R. L. Jones, C. W. Litton, G. Cantwell, and W. C. Harsch, Solid State Commun. **105**, 399 (1998).
[39]O. Bierwagen and J. S. Speck, Appl. Phys. Lett. **101**, 102107 (2012).
[40]H. Ehrenreich, Phys. Rev. **120**, 1951 (1960).
[41]H. Sobotta, H. Neumann, G. Kühn, and V. Riede, Cryst. Res. Technol. **25**, 61 (1990).
[42]K. J. Bachmann, F. S. L. Hsu, and J. P. Remeika, Phys. Status Solidi A **67**, K39 (1981).
[43]C. Weissmantel and C. Hamann, *Grundlager der Festkörperphysik* (VEB Deutscher Verlag der Wissenschaften, Berlin, 1979).
[44]J. Singh, *Physics of Semiconductors and their Heterostructures* (McGraw-Hill, New York, 1993).
[45]J. Singh (private communication).
[46]H. Ehrenreich, J. Phys. Chem. Solids **8**, 130 (1959).
[47]*Handbook of Transparent Conductors*, edited by D. Ginley (Springer, New York, 2010).
[48]H. Ehrenreich, J. Appl. Phys. **32**, 2155 (1961).
[49]R. L. Weiher and R. P. Ley, J. Appl. Phys. **37**, 299 (1966).
[50]N. G. Nilsson, Phys. Status Solidi A **19**, K75 (1973).
[51]V. Scherer, C. Janowitz, A. Krapf, H. Dwelk, D. Braun, and R. Manzke, Appl. Phys. Lett. **100**, 212108 (2012).
[52]H. Fujiwara and M. Kondo, Phys. Rev. B **71**, 075109 (2005).
[53]K. H. L. Zhang, R. G. Egdell, F. Offi, S. Iacobucci, L. Petaccia, S. Gorovikov, and P. D. C. King, Phys. Rev. Lett. **110**, 056803 (2013).